Article

Novel hydrophobic slippery surface-based SERS platform for ultra-sensitive detection in food safety

Dongjie Zhang, Hongjun You, Lei Yuan, Rui Hao, Tao Li, and Jixiang Fang

Anal. Chem., **Just Accepted Manuscript** • DOI: 10.1021/acs.analchem.9b00085 • Publication Date (Web): 27 Feb 2019

Novel hydrophobic slippery surface-based SERS platform for ultra-sensitive detection in food safety

Dongjie Zhang[1], Hongjun You[2], Lei Yuan[3], Rui Hao[1], Tao Li[3,*], Jixiang Fang[1,*]

[1.] *Key Laboratory of Physical Electronics and Devices of Ministry of Education, School of Electronic and Information Engineering, Xi'an Jiaotong University, Xi'an, Shann xi, 710049, China*

[2.] *School of Science, Xi'an Jiaotong University, Xi'an, Shann xi, 710049, China*

[3.] *Shaanxi Institute for Food and Drug Control, Xi'an, Shaanxi, 710065, China*

ABSTRACT: Collecting highly diluted target analytes into specific hot spot regions is vital for ultra-sensitive surface-enhanced Raman spectroscopy (SERS) applications. In this work, a hydrophobic slippery platform was designed as a concentrator to construct colloidal SERS-active substrates regardless of the diffusion limits during droplet evaporation. Within only 140 s, sufficient absorption between the analytes and colloidal Au nanoparticles (Au NPs) was observed by fluorescence imaging. This effect resulted in excellent SERS sensitivity and stability. Compared with the common metal colloid-based SERS substrates, such as drying on a silicon wafer or detecting in colloidal solutions, this pre-concentrated method showed lower detection limits and lowest concentration of crystal violet molecule down to 10^{-12} M with a portal Raman spectrometer. Such high signal enhancement was mainly ascribed to the condensation effect of Au colloids/analytes on the hydrophobic slippery substrate, by which almost all probe molecules were guided into the "hot spot" regions of aggregated Au NPs. Based on the SERS platform, various illegal additives in realistic food and health-care products, e.g., malachite green (1 ppb) added in fish and morphine (0.1 ppm) added in chafing dish, could be sensitively detected. Therefore, our protocol is a general SERS platform that may provide a simple, fast and cost-effective approach for trace molecular sensing.

* To whom correspondence should be addressed. E-mail: jxfang@mail.xjtu.edu.cn; westyx@126.com

INTRODUCTION

Food safety issues, such as the Malachite Green (MG) incident, Sudan red duck eggs, and poisonous milk powder with melamine, seriously harm the public health and have recently incited worldwide concern.[1,2] Surface-enhanced Raman spectroscopy (SERS) has attracted considerable attention since its discovery in 1974 and has been applied to various fields, such as electrochemistry, catalysis, bio-sensing, food safety, and environmental monitoring due to its high sensitivity, effective selectivity, label-free detection and unique spectroscopic fingerprint.[3-8] SERS detection involves the interactions among incident light, plasmonic nanostructures, and probe molecules, especially the interaction between light and nanostructures based on LSPR effects. In the last decade, extensive studies have focused on the preparation of optimized SERS substrates with high density of "hot spots" to obtain enhanced signals. Various nanostructures have been precisely controlled with measured sizes, controlled morphologies, and inner gaps.[9-12] Among them, metal colloid-based SERS substrates have been widely used for practical detections because of their easy sample preparation, low cost, ease of manipulation, and high sensitivity.

However, SERS detection is a relatively complicated system. The absorption effects between target molecule and plasmonic nanostructure play an important role in the ultrasensitive SERS detection. Therefore, concentrating probe molecules into the intensive hot spot regions is vital for SERS sensitivity, stability, and reproducibility. Many factors, such as surface energy and tension, colloidal NP size and shape, droplet shape, and colloidal surface charges influence the final patterns and SERS performances during droplet evaporation.[13-19] Unfortunately, the molecules and colloidal NPs dispersed in solutions freely diffuse over the surfaces during evaporation, resulting in poor molecular accessibility to plasmonic sensitive regions. Thus, a large proportion of analytes cannot be efficiently excited by the enhanced near-fields. Super-hydrophobic membranes are a useful method to drive molecules into the sensitive region and

consequently enhance the SERS signals.[20-22] However, most reported super-hydrophobic SERS substrates require various nanofabrication apparatus, such as E-beam lithography, optical lithography, and reactive ion etching, thus increasing the cost for real SERS applications.

Here, a simple, time-saving, and reliable SERS substrate was introduced to enrich and deliver analytes into specific sensitive sites based on a hydrophobic slippery surface. This pinning-free substrate was simply prepared by infusing perfluorinated fluid into the hydrophobic PTFE membrane to eliminate the diffusion limit during droplet evaporation. Fluorescence imaging analysis showed that the detected molecules tend to be concentrated on the surface and into the gaps of aggregated Au NPs with enhanced electric field. As a result, the SERS signals of CV molecule could be detected as low as 10^{-12} M with 23% probability, showing advantages over the common colloidal SERS substrates. Moreover, various illegal additives in food and health-care products, e.g., MG added in fish and morphine added in chafing dish, were sensitively detected on the slippery substrate, thereby showing huge potential for practical applications.

EXPERIMENTAL SECTION

Materials. $HAuCl_4 \cdot 4H_2O$ (99.9%) and trisodium citrate ($Na_3C_6H_5O_7 \cdot 2H_2O$, 99%) were purchased from Sigma Aldrich. Teflon membrane (polytetrafluoroethylene, PTFE) with 0.1 μm pore size and 70 μm thickness was purchased from Whatman Corporation. Perfluorinated fluids (Krytox, GPL 105) were purchased from Dupont Corporation. All illegal additives and real samples, e.g., crystal violet (CV), erythrosine, malachite green (MG), sildenafil, and clonidine hydrochloride, were obtained from Shaanxi Institute for Food and Drug Control. All chemicals were used without any further purification. Millipore Ultrapure water with 18.2 MΩ was used in all experiments.

Synthesis of Au NPs with different sizes. Small Au NPs with 30 nm in diameter were synthesized based on a modified citrate reduction approach.[23] In brief, 100 mL of 0.2 mM

aqueous $HAuCl_4$ solution was placed into a conical flask with oil bath. After the solution has boiled, 8 mL of 1%wt sodium citrate solution was added immediately under magnetic stirring (500 rpm). The solution tuned to wine red color after 15 min. After a complete reaction for further 45 min, colloidal Au NPs were obtained and then stored in 4 °C. Au NPs with 55 nm in diameter could be obtained by adjusting the content of added gold precursor and reducing agent. The concentration of aqueous $HAuCl_4$ increased from 0.2 mM to 0.25 mM, whereas the dosage of sodium citrate solution (1 %wt) reduced form 8 mL to 0.8 mL.

Large sized Au NPs with ~80 nm were prepared based on a seed-mediated growth method. The above Au NPs with 30 nm were used as the nanoseeds. As shown in Table 1, the growth process of large gold nanoparticles includes three steps to obtain uniform shape and size distribution. For growth step 1, 80 mL of ultrapure water and 20 mL of Au seeds were mixed into a three-neck flat-bottom flask and heated to boil. Then, 2 mL of sodium citrate solution (1 %) was injected immediately, and 0.2 mL of $HAuCl_4$ was added 5 min later. Additional 0.2 mL dosage of $HAuCl_4$ was needed for nine times. The reaction time between every two injections was 5 min. After the last precursor was added, the reaction should last for 30 min. Au colloids prepared in step 1 were used as the seed solution, and the growth process was repeated twice for growth steps 2 and 3. $HAuCl_4$ was added for eight times for step 3. Finally, Au colloids with 80 nm in diameter were prepared with a brick red color. Figure S1 showed the size distributions of Au NPs with approximate 30, 55, and 80 nm in diameter. The UV-Vis absorbance spectra of various Au Colloids indicated that the corresponding absorbance peaks were located at 525, 536, and 548 nm (Figure S2), which was in accordance with the previous report[23].

Table1 Experimental parameters for the growth of monodispersed Au NPs

Growth steps	H_2O (mL)	SC (1%)	Total $HAuCl_4$ (10 mM)	Adding times	Dosage (mL)
Step 1	80 ml	2 ml	2 ml	10	0.2 ml
Step 2	80 ml	2 ml	2 ml	10	0.2 ml
Step 3	80 ml	2 ml	1.6 ml	8	0.2 ml

Preparation of SERS Substrates. The colloidal Au NPs were used as SERS-active nanoparticles. Concentrated molecules and NPs were prepared on a hydrophobic slippery Teflon membrane as follows: first, a Teflon membrane was attached on a flat glass slide (5cm×5 cm) by using a double-sided adhesive. Then, 0.45 mL of perfluorinated fluid was dispersed by spin coating. The low speed was 600 rpm for 30 s, and the high speed was 1500 rpm for 1 min. After the excess lubricating liquid was removed, the infused membrane was heated for 30 min and obtained for further use. Lastly, 50 μL of probe molecules and 10 μL of Au colloids were simultaneously dropped onto the slippery surface. During drying, the contact line shrunk due to the low friction of the lubricated Teflon surface. As a result, the initial droplet could be concentrated into a small area with less than 0.5 mm. Instead of hydrophobic slippery membrane, a common silicon wafer was used as the support surface for the evaporation of Au colloids and analytes. Moreover, SERS signals could also be collected by using an optical fiber focused on the mixed solution of samples.[24]

Finite difference time-domain (FDTD) simulation. The electromagnetic field intensity distribution of the closely packed Au NPs was studied by FDTD simulation. The incident light was a plane wave propagating from the left to the right along x axis, and the excitation wavelengths were 532, 633, and 785 nm. The monitor was set at the y-z plane facing the light source, and the mesh size was 2 nm × 2 nm × 2 nm. As shown in Figure S7, the distance between Au NPs (4×4×4 array) was 2 nm. The diameters of Au NPs

were 30, 55, and 80 nm according to the real nanoparticle sizes in the experiment.

Pretreatment of additives in realistic food and health-care products. A certain pretreatment process was necessary to achieve SERS detection of illegal additive molecules. Real samples of fish, chafing dish, and health-care products were obtained from Shaanxi Institute for Food and Drug Control. The fish and health-care samples were mashed first, and then 2 g of each sample was added into 10 mL of methanol solvent. The mixture was ultrasonically mixed for 10 min and then centrifuged at 4000 rpm for 5 min to remove impurities and macromolecular protein. The upper solution was extracted and dispersed in methanol again. The processes of ultrasonic mixing and centrifugation were repeated for four times. Finally, the obtained sample was further purified by 0.22 μm filter membrane and then adjusted to 10 mL volume for practical Raman test.

Characterization. The morphology and structure of samples were characterized by scanning electron microscope (SEM, FEI, Quanta 250 FEG) and transmission electron microscope (TEM, JEOL, JEM-2100F with an accelerating voltage of 100 kV). Optical properties were characterized using an ultraviolet–visible spectroscopy (Aglient, Carry 60). Contact angle was measured on an optical contact angle instrument (KRUSS, DSA 100). Bright-field and fluorescence imaging was conducted on a self-made optical testing platform in our laboratory with a mercury lamp as the excited source. Comparison of SERS detection with various excited laser wavelengths (532, 633 and 785 nm) was also conducted on the optical testing platform. SERS signals with real samples were measured on a portable Raman spectrometer (BWTEK, i-Raman) with a 785 nm laser. The exposure time was 20 s, and the laser power was 5% (approximately 30 mW).

RESULTS AND DISCUSSION

Droplet evaporation is a common daily phenomenon. However, the physical mechanism of evaporation is quite complicated and involves heat releasing and particle deposition. Understanding and controlling the evaporation of droplets is important for a wide range of applications, including inkjet printing, electronic chip cooling, water harvest, and biosensing.[25-27] Based on contact line dynamics, evaporation could be included as three classes[28,29]: (1) constant contact angle (CCA) mode, (2) constant contact line (CCL) mode, and (3) a mixed mode. In most cases, coffee ring patterns, which could be ascribed for the pinning effects of contact line and capillary flowing from the center to the margin of droplet, would be obtained during evaporation.[30]

To date, many studies have focused on the droplet evaporation and elimination of coffee ring effects.[31-35] Researchers showed that the shapes of colloidal NPs could affect the formation of coffee ring patterns.[13] Colloidal NPs with anisotropic shapes were likely to locate at the gas–liquid interface, instead of gas–liquid–solid interfaces, leading to a uniform deposition during droplet evaporation. In addition, Weon[14] found that the sizes of colloidal NPs play an important role in droplet evaporation due to the effects of capillary force. Large nanoparticles are easily deposited in the central regions. Moreover, the droplet size could also affect the deposited patterns. When the size of droplet is small, the evaporation rate is faster than the moving rate of colloidal NPs, resulting in the disappearance of coffee ring patterns.[15]

Based on the above research, a hydrophobic slippery platform was designed by spin coating the perfluorinated liquid on PTFE membrane. Given its low surface tension, the perfluorinated membrane was immiscible for aqueous and organic samples. Moreover, the Teflon membranes were cheap and available from the market. We used colloidal Au NPs as SERS-enhanced materials. As shown in Figure 1, the preparation of SERS substrates was simple via directly depositing a droplet of Au NPs and probe molecule on the slippery surface. During solvent evaporation, the contact line slid due to the low

friction of the lubricated Teflon surface. Finally, the diluted analytes can be concentrated in a small area located at the surface or the nanogaps of aggregated Au NPs. This drying-mediated condensation provides a desirable platform for practical SERS detection.

As shown in Figure 2a, 10 μL of colloidal Au NPs and 50 μL of CV molecules (10^{-10} M) were dropped on the slippery surface. During evaporation, the color changed from transparent to dark black (the right image in Fig 2b), indicating the increased concentration of Au NPs/CV. The droplet diameter reduced from approximately 0.85 cm to the final 0.2 mm as shown in the left image in Fig 2b. In addition, the droplet mobility on slippery surface was influenced by solvents, perfluorinated fluids, and evaporation rate. In particular, the droplet size and evaporation rate played an important role for the enrichment efficiency. Figure S3 shows the SERS spectra of CV molecules (10^{-10} M) with different evaporation temperatures (60 °C–160 °C). Considering the signal intensity and evaporation time, 140 °C was selected as the optimal temperature under which SERS substrate could be prepared within 140 s. Four pieces of slippery membranes with different batches were prepared to evaluate the stability of enrichment effects, and four Au/CV droplets were added on each surface. As shown in Figure S4, almost all droplets could be effectively controlled into a small region within 0.5 mm, indicating good reproducibility. Figures 2c and 2e show the evolution of contact angle and contact line with different evaporation stages. During evaporation, the droplet volume and contact area decreased gradually, and the pinning effect was nearly eliminated. Here, the process of droplet evaporation followed a constant contact angle mode, indicating that the receding contact angle was stable during evaporation. The last image in Figure 2e further confirms that the final size of Au NPs was less than 1 mm at 130 s. Figure 2d shows the SEM image of concentrated Au NPs on the slippery surface. The monodispersed citrate stabilized Au colloids were prepared based on a seed-mediated growth method. The aggregated Au NPs with tiny inter-particle gaps (less than 5 nm) may provide abundant hot spots, resulting in the enormous SERS enhancement.

Fluorescence imaging integrated with Raman spectra were employed to locate target regions and obtain SERS signal based on a self-made optical testing system in our laboratory to investigate the adsorption behavior of Au NPs and analytes on the slippery substrates. CV was selected as the probe molecule and showed a characteristic red color by fluorescence imaging (Figure S5). As a result, the detected molecules could be located immediately via fluorescence images. Figures 3a and 3b presented the bright field and fluorescence images of 10^{-9} M CV molecules absorbed on the Au aggregates. The results indicated that almost all molecules had been guided to the surface and gap regions of Au NPs. No fluorescence signal could be found in the surrounding regions (region 1, 2 or 3 in Figure 3b) when the droplet diameter reduced from approximately 0.85 cm to the final 0.2 mm. The analytes distribution could be observed in the insets with high resolutions in Figure 3c. Moreover, Figure S6 shows the fluorescence images of diluted CV molecules with 10^{-10} M, indicating an intensity decline. Figure 3c shows the SERS spectra of 10^{-9} M CV molecules, indicating that Raman signals are likely to be recorded at the center of aggregated spots. The main vibrational peaks of CV molecules were located at 727, 808, 914, 1173, 1388, 1530, 1586, and 1617 cm^{-1}. The enhanced SERS signals originated from the thorough adsorption of analytes and aggregated Au NPs. However, when the laser spot focused on the surrounding region (marked by the black arrow in Fig 3c insets), the Raman signal almost disappeared. This finding implied that only few Au NPs were located at the outer areas. In summary, the differences of SERS signals indicated that probe molecules should be concentrated at the specific hot spot regions to achieve sensitive SERS detection.

The SERS performance of colloidal Au NPs was evaluated with different NP sizes and laser wavelengths based on the slippery surface. Small sized Au NPs with 30 \and 55 nm in diameter (Figure 4a and 4c, Figure S1) were prepared by controlling the added amounts of Trisodium citrate and $HAuCl_4$ solutions. The FDTD simulation (Figures 4b, 4d, 4f, and S8) showed the electromagnetic enhancement of various Au NPs under 532,

633, and 785 nm excited laser. The results showed that 80 nm Au NPs exhibited the strongest electromagnetic enhancement under 785 nm laser compared with the small-sized Au NPs. Raman spectra of 30 points were acquired randomly for each sample, and characteristic band around 1173 cm^{-1} was used to count the average Raman intensity (I_{ave}). The compared SERS spectra of CV molecule also confirmed that the optimized conditions were 80 nm Au NPs and 785 nm laser wavelength (Figures 4g and S9–S11). Raman spectra of CV molecules with a series of concentrations (10^{-7} M to 10^{-13} M) were also measured to explore the detection limit of target molecule. As shown in Figure 4h, all characteristic Raman peaks could be distinguishable even at a concentration of 10^{-11} M. When the concentration was reduced to 10^{-12} M, the SERS signal could still be recognized by amplifying SERS intensity for 10 times, showing extremely low SERS detection limit. The reproducibility was also important for active SERS substrates. Forty spots of Raman signals were measured for 10^{-10} M, 10^{-11} M, and 10^{-12} M CV to test the reproducibility performance. In the collective Raman spectra shown in Figure S12, the occurrence probability of 10^{-10} M CV was 100%. When the concentration was reduced to 10^{-11} M, the probability of detected Raman signals was reduced to ~60%. Even for the ultra-low 10^{-12} M, the probability to receive observable SERS signals remained at ~ 23%.

Detection in colloidal solutions (Route 1) or on silicon wafer (Route 2) is the common method for metal colloid-based SERS substrates as shown in Figure 5. Here, these two methods were employed to detect CV molecules with 10^{-10} M and compare them with concentrated Au/analytes on slippery surface (Route 3). For Route 1, a certain amount of NaCl was introduced to the Au colloids and molecules, resulting in the aggregation of nanoparticles. The ionic-induced colloid aggregation could provide abundant junction sites and thus produce intense SERS signals.[36,37] For Route 2, silicon wafer was employed as the support for droplet evaporation. As shown in Figure S13, the receding contact angle θ_R for the silicon wafer was low (~17°) during evaporation,

whereas the θ_R for the hydrophobic slippery surface was 53°. In particular, the value of θ_R greatly influenced the particle aggregation during evaporation, and an increased θ_R would result in a closed-packed assembling.[38,39] As a result, the ‘‘coffee-ring’’ pattern occurred on the silicon wafer, leading to the random distribution of molecules and Au NPs as reported in our previous work.[40] The right graph in Figure 5 illustrates that the route 3 on hydrophobic slippery surface showed the most enhanced SERS signal, and the detection on silicon wafer exhibited the lowest Raman intensity.

Additional probe molecules were detected by different methods, and their respective chemical structures were described in the insets in Figure 6 to verify the detection advantage of hydrophobic slippery substrates. Table S1 revealed the detection limits of various illegal molecules in food additives and health-care products by different methods. With the use of hydrophobic slippery surface-based SERS platform, the lowest detection concentrations of MG, erythrosine, sildenafil, and clonidine hydrochloride were 0.0036 ppb, 0.4 ppb, 0.01 ppm, and 0.02 ppm, respectively. However, the lowest detection concentrations of these four analytes by Route 2 were only 1 ppb, 0.1 ppm, 0.1 ppm, and 2 ppm (Figures S14b, S14e, S15b, and S15e). For Route 1, the lowest detection concentrations of MG, erythrosine, and clonidine hydrochloride were 1 ppb, 0.01 ppm, and 50 ppm, respectively. The measurement in solution showed no signal of sildenafil even at 1000 ppm due to the influence of ethanol solvent, indicating that detection Route 1 was only suitable for aqueous samples (Figure S14a, S14d, S15a, and S15d). Comparison of SERS detection limits indicated that hydrophobic slippery platform has good signal sensitivity, thus verifying the Raman spectra of CV molecules in Figure 5.

To reveal the potential applications of hydrophobic slippery surface-based SERS substrate, we detected some illegal additives in realistic food and health-care products, e.g., MG added in fish, morphine added in chafing dish, and two kinds of sildenafil added in health-care products. Here, this SERS-based detection showed some advantages compared with the other methods, such as HPLC-MS. The pretreatment process was

much easier. For example, for the pretreatment of morphine in chafing dish, only ultraphonic mixing, centrifugation and filtration were needed for SERS detection, and methanol solvent was the only added reagent in the whole process. However, for HPLC-MS, the pretreatment process involved ultraphonic mixing, centrifugation, vortex oscillation and filtration, and various reagents, such as acetonitrile, magnesium sulfate, sodium acetate, etc., were needed. Moreover, the operation was much simple and the detection time was shorter for SERS detection. Only 140s was needed for the droplet evaporation and 20s for spectra collection in Raman test. However, for HPLC-MS, the standard operation procedure was complicated, and at least 10 min was needed.

As a prohibited food additive, MG was often used in aquaculture due to its low cost and effective antibacterial activity.[41] As shown in Figure 7a, the characteristic bands at 796, 1367, 1584, and 1613 cm^{-1} were ascribed to MG molecules and could be identified even at a concentration as low as 1 ppb. In addition, the lowest concentration of morphine was 0.1 ppm for the recognition of 628, 757, 1030, and 1581 cm^{-1} bands (Figure 7b).[42] As an illegal additive, sildenafil was often mixed into the health-care food as an anti-fatigue component. Here, the lowest detection concentrations of sildenafil in the two kinds of health-care product samples were down to 0.076 and 0.124 ppm (Figure 7c and 7d). The sensitive detection of different additives indicated the possible application of the hydrophobic slippery platform on real-world SERS detection.

CONCLUSION

We have presented a rapid, convenient, and cost-effective method to synthesize active SERS substrates with the aid of hydrophobic slippery surface and the use of common Au colloids as enhanced materials. During evaporation, almost all target molecules could be delivered into the “hot spot” regions of aggregated Au NPs due to the condensation effect of infused Teflon films. The droplet size could be reduced from approximately 0.85 cm to less than 0.5 mm within only 140 s, showing remarkable

condensing efficiency. By employing a portable Raman spectrometer, the proposed method exhibited excellent SERS sensitivity and reproducibility, and the lowest concentration of CV molecule could be achieved at 10^{-12} M, showing advantages over the common colloid-based SERS substrates. Furthermore, several illegal additives in realistic food and health-care products with low concentrations could be detected rapidly by this method, implying its potential SERS applications for rapid, portable, and sensitive trace molecular sensing.

ASSOCIATED CONTENT

Supporting Information

The Supporting Information is available free of charge on the ACS Publications website at DOI:

Size distribution of Au NPs, UV-Vis spectra of colloidal Au NPs, SERS spectra of CV under different evaporation temperatures, optical and fluorescent imaging of concentrated Au/CV aggregates, FDTD simulation model and results of Au NPs, SERS spectra of CV with various laser, the receding contact angles of droplets, and SERS detection of illegal molecules in food safety.

AUTHOR INFORMATION

Corresponding Authors

*E-mail: jxfang@mail.xjtu.edu.cn; westyx@126.com. Tel: +86-82668150

ACKNOWLEDGMENTS

J. X. Fang acknowledges the programs supported by the National Natural Science Foundation of China (No. 21675122, 21874104), the Key Research Program in Shaanxi (2017NY-114), the World-Class Universities (Disciplines) and the Characteristic Development Guidance Funds for the Central Universities.

REFERENCES

(1) Duncan, T. V. *J Colloid. Interf. Sci.* **2011**, *363*, 1-24.

(2) Yaseen, T.; Pu, H.; Sun, D.W. *Trends. Food. Sci. Tech.* **2018**, *72*, 162-174.

(3) Schlucker, S. *Angew. Chem., Int. Ed.* **2014**, *53*, 4756-4795.

(4) Liu, Z.; Yang, Z.; Peng, B.; Cao, C.; Zhang, C.; You, H.; Xiong, Q.; Li, Z.; Fang, J. *Adv. Mater.* **2014**, *26*, 2431-2439.

(5) Chen, H. Y.; Lin, M. H.; Wang, C. Y.; Chang, Y. M.; Gwo, S. *J. Am. Chem. Soc.* **2015**, *137*, 13698-13705.

(6) Liu, Z.; Cheng, L.; Zhang, L.; Yang, Z.; Liu, Z.; Fang, J. *Biomaterials* **2014**, *35*, 4099-4107.

(7) Xie, X.; Pu, H.; Sun, D.W. *Crit. Rev. Food. Sci.* **2017**, 1-14.

(8) Pu, H.; Xiao, W.; Sun, D.-W. *Trends. Food. Sci. Tech.* **2017**, *70*, 114-126.

(9) Fang, J.; Du, S.; Lebedkin, S.; Li, Z.; Kruk, R.; Kappes, M.; Hahn, H. *Nano. Lett.* **2010**, *10*, 5006-5013.

(10) Zhang, D.; Zhang, C.; Lu, Y.; Hao, R.; Liu, Y.; Hao, Y. *J. Nanosci. Nanotechno.* **2017**, *17*, 2191-2195.

(11) Zhou, B.; Mao, M.; Cao, X.; Ge, M.; Tang, X.; Li, S.; Lin, D.; Yang, L.; Liu, J. *Anal. Chem.* **2018**, *90*, 3826-3832.

(12) Lu, H.; Zhu, L.; Zhang, C.; Chen, K.; Cui, Y. *Anal. Chem.* **2018**, *90*, 4535-4543.

(13) Yunker, P. J.; Still, T.; Lohr, M. A.; Yodh, A. G. *Nature* **2011**, *476*, 308-311.

(14) Weon, B. M.; Je, J. H. *Phys. Rev. E.* **2010**, *82*, 015305.

(15) Shen, X.; Ho, C.-M.; Wong, T. S. *J. Phys. Chem. B.* **2010**, *114*, 5269-5274.

(16) Chen, X.; Ma, R.; Li, J.; Hao, C.; Guo, W.; Luk, B. L.; Li, S. C.; Yao, S.; Wang, Z. *Phys. Rev. Lett.* **2012**, *109*, 116101.

(17) Sun, J.; Bao, B.; He, M.; Zhou, H.; Song, Y. *ACS. Appl. Mater. Inter.* **2015**, *7*, 28086-28099.

(18) Zhang, Y.; Yang, S.; Chen, L.; Evans, J. R. G. *Langmuir* **2008**, *24*, 3752-3758.

(19) Zhang, Y.; Evans, J. R. G. *J Colloid. Interf. Sci.* **2013**, *395*, 11-17.

(20) Shin, S.; Lee, J.; Lee, S.; Kim, H.; Seo, J.; Kim, D.; Hong, J.; Lee, S.; Lee, T. *Small* **2017**, *13*, 1602865.

(21) De Angelis, F.; Gentile, F.; Mecarini, F.; Das, G.; Moretti, M.; Candeloro, P.; Coluccio, M. L.; Cojoc, G.; Accardo, A.; Liberale, C.; Zaccaria, R. P.; Perozziello, G.; Tirinato, L.; Toma, A.; Cuda, G.; Cingolani, R.; Di Fabrizio, E. *Nat. Photonics.* **2011**, *5*, 682-687.

(22) Jayram, N. D.; Aishwarya, D.; Sonia, S.; Mangalaraj, D.; Kumar, P. S.; Rao, G. M. *J Colloid. Interf. Sci.* **2016**, *477*, 209-219.

(23) Bastus, N. G.; Comenge, J.; Puntes, V. *Langmuir* **2011**, *27*, 11098-11105.

(24) Yang, Q.; Liang, F.; Wang, D.; Ma, P.; Gao, D.; Han, J.; Li, Y.; Yu, A.; Song, D.; Wang, X. *Anal. Method.* **2014**, *6*, 8388-8395.

(25) Park, J.; Moon, J. *Langmuir* **2006**, *22*, 3506-3513.

(26) Layani, M.; Gruchko, M.; Milo, O.; Balberg, I.; Azulay, D.; Magdassi, S. *ACS Nano* **2009**, *3*, 3537-3542.

(27) Smalyukh, II; Zribi, O. V.; Butler, J. C.; Lavrentovich, O. D.; Wong, G. C. *Phys. Rev. Lett.* **2006**, *96*, 177801.

(28) Xu, W.; Leeladhar, R.; Kang, Y. T.; Choi, C. H. *Langmuir* **2013**, *29*, 6032-6041.

(29) Arcamone, J.; Dujardin, E.; Rius, G.; Pérez-Murano, F.; Ondarçuhu, T. *J. Phys. Chem. B.* **2007**, *111*, 13020-13027.

(30) Deegan, R. D.; Bakajin, O.; Dupont, T. F.; Huber, G.; Nagel, S. R.; Witten, T. A. *Nature* **1997**, *389*, 827.

(31) Li, Y. F.; Sheng, Y. J.; Tsao, H. K. *Langmuir* **2013**, *29*, 7802-7811.

(32) Li, P.; Li, Y.; Zhou, Z. K.; Tang, S.; Yu, X. F.; Xiao, S.; Wu, Z.; Xiao, Q.; Zhao, Y.; Wang, H.; Chu, P. K. *Adv. Mater.* **2016**, *28*, 2511-2518.

(33) Deegan, R. D.; Bakajin, O.; Dupont, T. F.; Huber, G.; Nagel, S. R.; Witten, T. A.

Nature **1997**, *389*, 827-829.

(34) Anyfantakis, M.; Geng, Z.; Morel, M.; Rudiuk, S.; Baigl, D. *Langmuir* **2015**, *31*, 4113-4120.

(35) Anyfantakis, M.; Baigl, D. *Angew. Chem., Int. Ed.* **2014**, *53*, 14077-14081.

(36) Xu, L. J.; Lei, Z. C.; Li, J.; Zong, C.; Yang, C. J.; Ren, B. *J. Am. Chem. Soc.* **2015**, *137*, 5149-5154.

(37) Lawson, L. S.; Chan, J. W.; Huser, T. *Nanoscale* **2014**, *6*, 7971-7980.

(38) Kuang, M.; Wang, J.; Bao, B.; Li, F.; Wang, L.; Jiang, L.; Song, Y. *Adv. Opt. Mater.* **2014**, *2*, 102-102.

(39) Dash, S.; Garimella, S. V. *Langmuir* **2013**, *29*, 10785-10795.

(40) Zhang, D.; Fang, J.; Li, T. *J Colloid. Interf. Sci.* **2018**, *514*, 217-226.

(41) Ai, Y. J.; Liang, P.; Wu, Y. X.; Dong, Q. M.; Li, J. B.; Bai, Y.; Xu, B. J.; Yu, Z.; Ni, D. *Food. Chem.* **2018**, *241*, 427-433.

(42) Vinesh, R.; Canamares, M. V.; Thomas, K.; Marco, L.; Lombardi, J. R. *J. Forensic. Sci.* **2011**, *56*, 200-207.

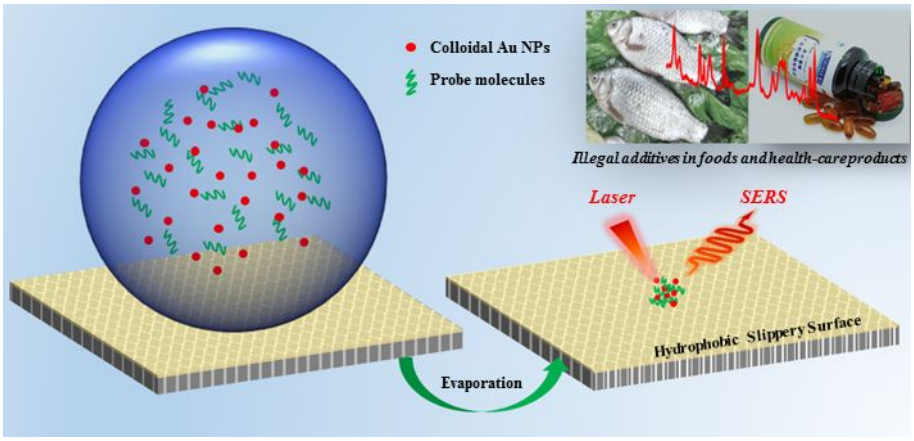

Figure 1. Schematic illustration of the SERS detection based on hydrophobic slippery surface.

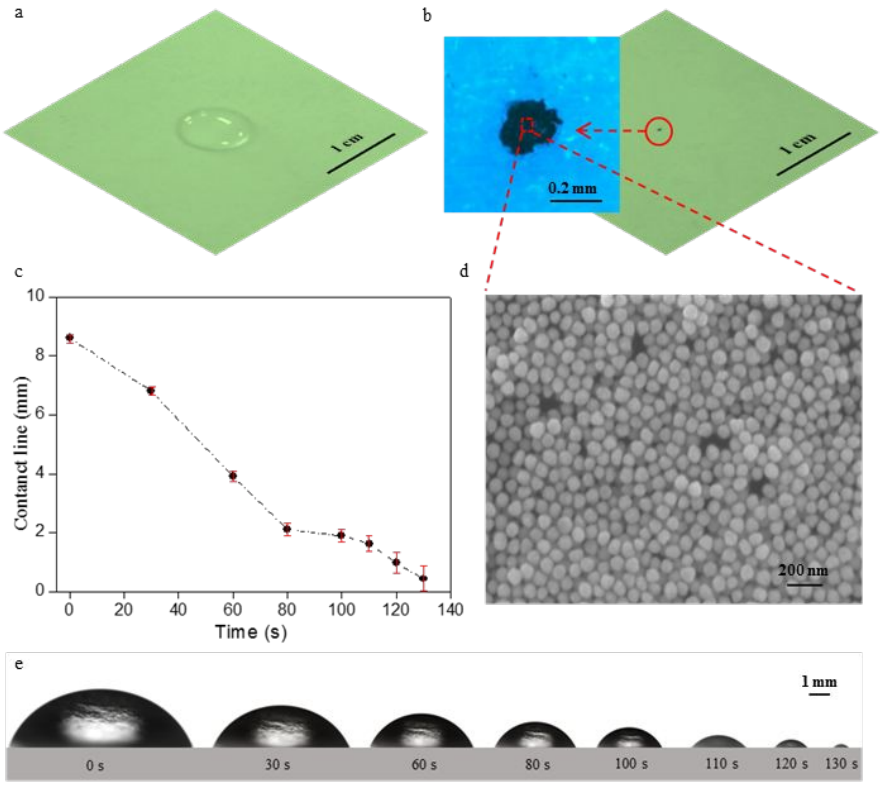

Figure 2. Evaporation process of Au NPs/analytes on the hydrophobic slippery surface characterized by optical imaging, SEM and contact angle. (a) The optical image of initial droplet on slippery surface, containing 10 μL Au colloids and 50 μL CV molecule (10^{-10} M). (b) The optical images of Au NPs/analytes after drying on slippery surface. The enlarged image leftwards was acquired by optical microscopy. (c) The time evolution of contact line during evaporation. (d) SEM image of concentrated Au NPs/CV extracted from the enlarged image in Fig. 2b. (e) The evolution of contact angle images during the evaporation. The optical images in Fig. 2a and Fig. 2b with low magnification taken by digital camera.

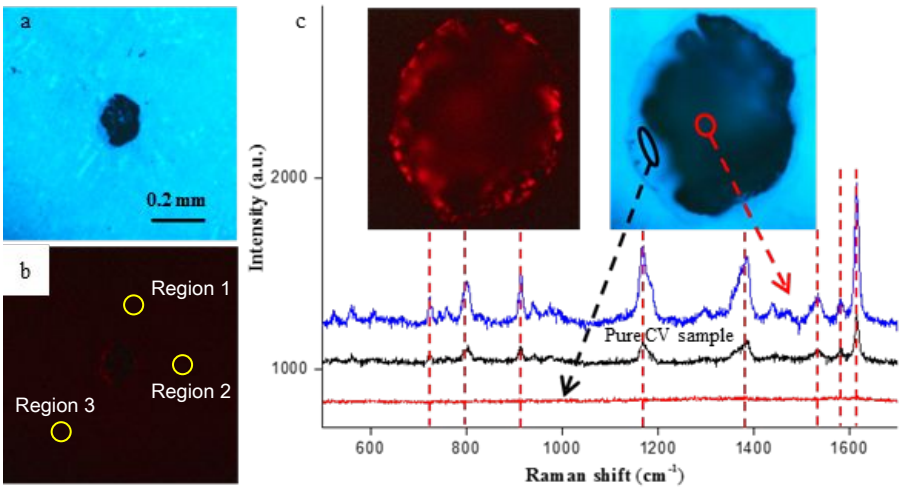

Figure 3. Fluorescent imaging and SERS detection of CV molecule with 10^{-9} M on hydrophobic slippery surface. (a) The bright-field optical imaging and (b) the fluorescent imaging with red color of concentrated Au NPs/molecule. (c) SERS spectra of CV molecule from different regions of aggregated Au NPs. The insets in Fig. 3c were optical and fluorescent images with high magnification extracted from Fig. 3a and Fig. 3b.

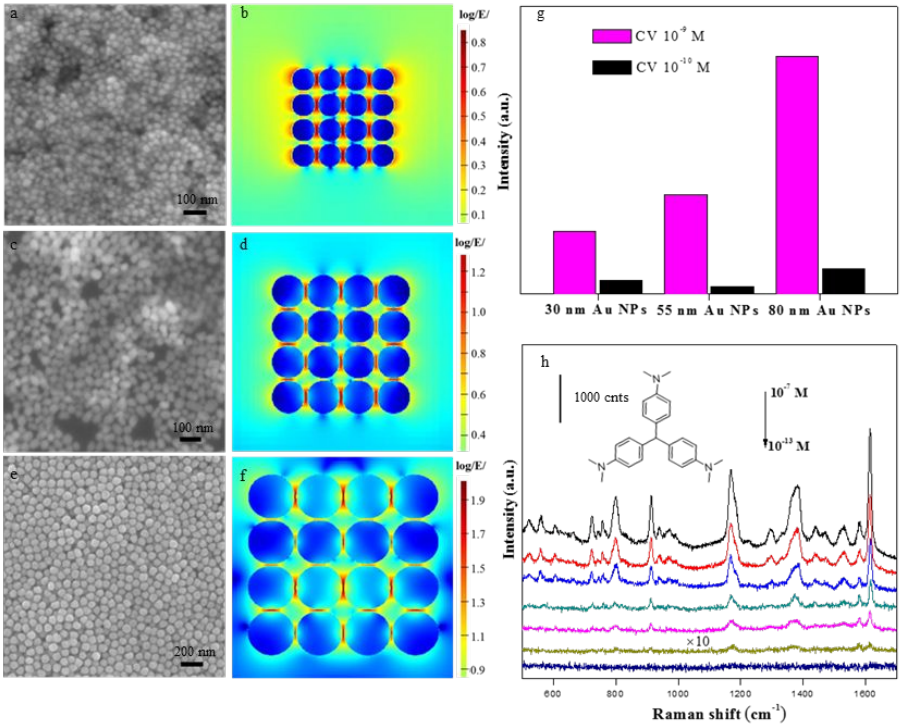

Figure 4. Characterization of aggregated Au NPs with various sizes, the electromagnetic enhancement and SERS spectra. The SEM images illustrated different Au NPs sizes: (a) 30 nm, (c) 55 nm and (e) 80 nm. The FDTD simulation showed the electromagnetic enhancement for various Au NPs: (b) 30 nm, (d) 55 nm and (f) 80 nm. (g) The averaged SERS intensity with different Au NPs

sizes. The concentrations of CV molecule were 10^{-9} M and 10^{-10} M. (e) The SERS spectra of CV molecule (10^{-7} M - 10^{-13} M) with 80 nm Au NPs. The laser wavelength was 785 nm.

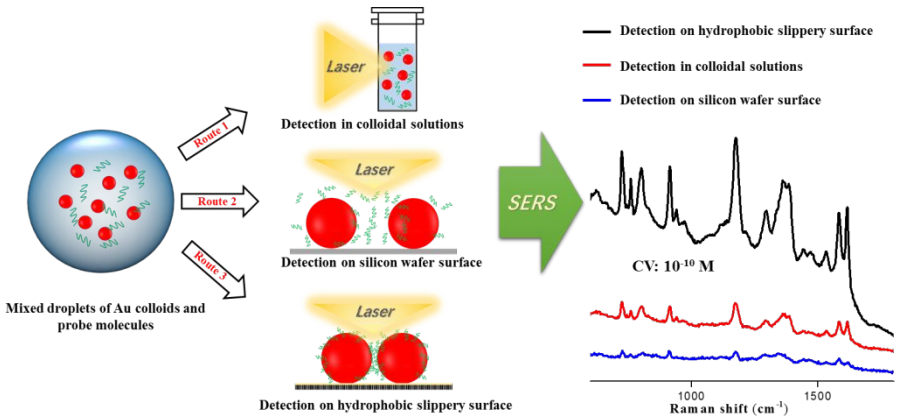

Figure 5. The schematic illustration of different SERS detection methods for metal colloids-based substrates. The SERS spectra in route 1was detected in colloidal solutions by adding NaCl as aggregation agent. The SERS spectra in route 2 and route 3 were collected on silicon wafer surface and hydrophobic slippery surface. The right figure showed the compared SERS spectra with 10^{-10} M CV molecule.

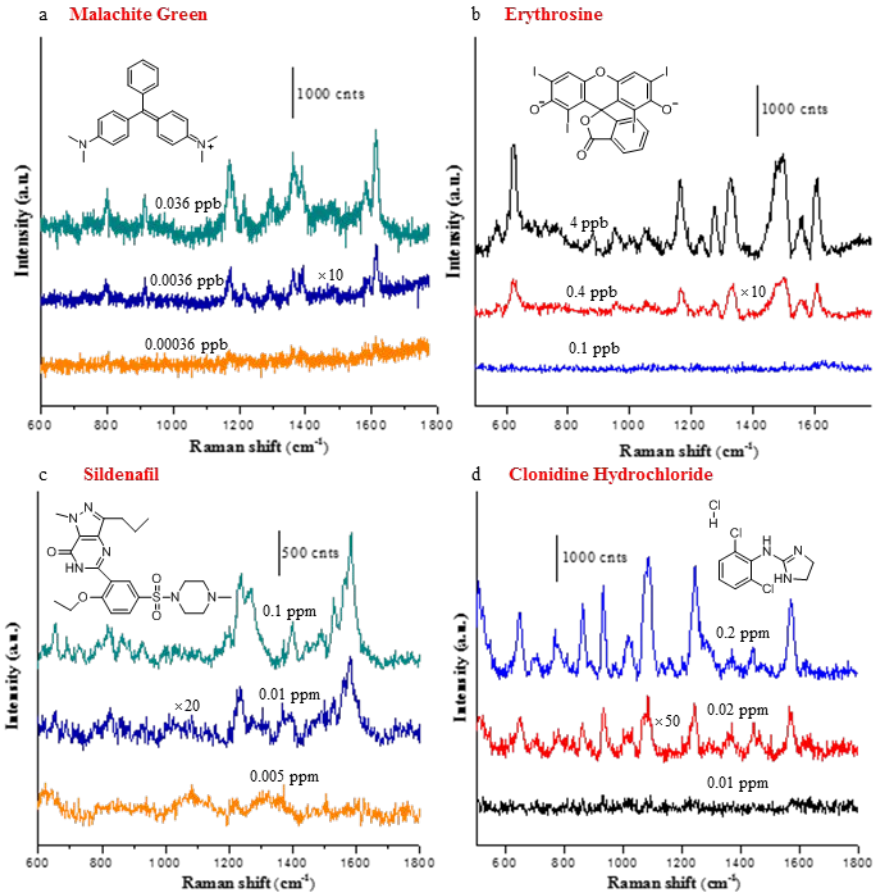

Figure 6. SERS detection of illegal additives. (a) SERS spectra of MG molecule. (b) SERS spectra of Erythrosine molecule. (c) SERS spectra of Sildenafil molecule. (d) SERS spectra of Clonidine hydrochloride molecule.

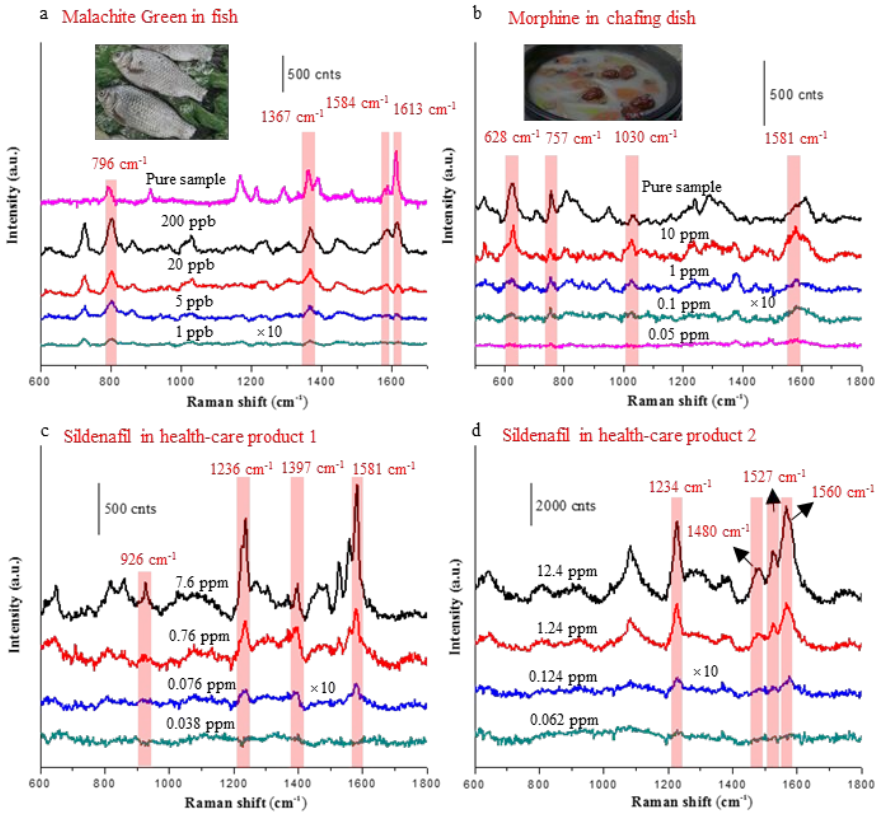

Figure 7. SERS detection of illegal additives in realistic food and health-care products. (a) SERS spectra of MG illegally added in fish. (b) SERS spectra of Morphine illegally added in chafing dish. (c)- (d) SERS spectra of sildenafil illegally added in different health-care products.

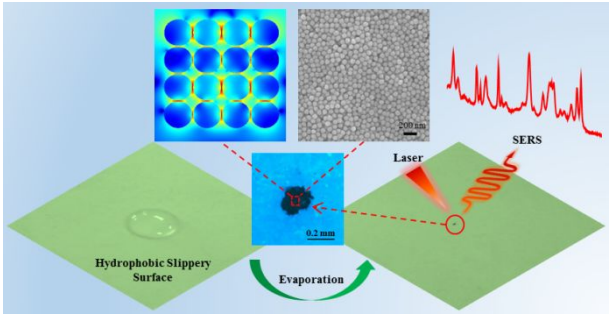

TOC Graphic